819

Research Report

Application of a Probabilistic Moment Tensor Inversion to Data Recorded above the Northgerman Gas Fields

DGMK

DGMK-Research Report 819

Application of a Probabilistic Moment Tensor Inversion to Data Recorded above the Northgerman Gas Fields

Abstract

Even if faults are not visible on geological outcrops, source mechanisms of earthquakes occurring on those faults may distinguish between different types of faulting. We implemented a novel, probabilistic full-waveform moment tensor inversion for the application to shallow micro-earthquakes close to gas fields in North Germany. Due to the probabilistic approach, parameter trade-offs, uncertainties and ambiguities are mapped. The implemented bootstrap method implicitly accounts for modelling errors that may affect every station and phase in a unique way. Furthermore, event locations are provided by the algorithm. Such hypocentres, which are estimated simultaneously with moment tensors, are often less sensitive to uncertainties in crustal structure. We analysed events from the November 20th, 2019, Kirchlinteln series as well as the October 1st, 2018 M_L 3.6 Lastrup event (00:28 UTC). We carefully investigated station quality, the usable frequency range, input data types, inversion parameters as well as velocity models and supplemented the analysis by a H/V study. The Kirchlinteln events show slightly oblique normal faulting and potentially, a complex faulting process involving several faults, fitting known local fault traces. The 00:28 UTC Lastrup event reveals thrust faulting, most likely on a single fault not fitting the regional fault trend.

DGMK-Forschungsbericht 819

Anwendung einer Probabilistischen Momententensorinversion auf Seismometer-Daten von Norddeutschen Erdgasfeldern

Kurzfassung

Auch wenn Verwerfungen nicht auf geologischen Aufschlüssen sichtbar sind, können die Quellmechanismen von auf diesen Verwerfungen stattfindenden Erdbeben helfen, die Art der Verwerfung zu bestimmen. In diesem Projekt nutzten wir eine neuartige, probabilistische Momententensorinversion vollständiger Wellenzüge, um Flachbeben mit geringen Magnituden in der Nähe der norddeutschen Gasfelder zu analysieren. Durch den probabilistischen Ansatz werden Parameterkonflikte, Unsicherheiten und Mehrdeutigkeiten abgebildet. Die verwendete Bootstrap-Methodik erlaubt es, Modellierungsfehler implizit zu berücksichtigen, die jede aufzeichnende Station und Wellenphase in unterschiedlichem Maß betreffen können. Zusätzlich liefert der Algorithmus Bebenhypozentren. Solche Hypozentren, die gleichzeitig mit dem Bebenmechanismus abgeschätzt werden, sind häufig weniger von Unsicherheiten in der Kenntnis der Krustenstruktur betroffen. Wir analysierten die Ereignisse der Kirchlinteln-Bebenserie am 20. November 2019 sowie das M_L 3.6 Lastrup Ereignis am 1. Oktober 2018 (00:28 UTC). Dazu untersuchten wir die Stationsqualitäten, den nutzbaren Frequenzbereich, verschiedene Eingabedatentypen, Inversionsparameter sowie Geschwindigkeitsmodelle und ergänzten die Arbeit mit einer H/V-Studie. Die Ereignisse bei Kirchlinteln zeigen eine leicht schräge Abschiebung und einen höchstwahrscheinlich komplexen Bruchprozeß unter Einbeziehung mehrerer bekannter, lokaler Verwerfungen. Das M_L 3.6 Ereignis bei Lastrup zeigt hingegen eine Schrägaufschiebung auf einer einzelnen Verwerfung, deren Ausrichtung nicht der regionalen Tendenz entspricht.

Table of Contents

Summary

Even if faults are not visible on geological outcrops, source mechanisms of earthquakes occurring on those faults may distinguish between different types of faulting. Moreover, the source mechanism of seismic events is one of the most important parameters to discriminate between natural and induced earthquakes and helps to understand the underlying cause. In addition, information on source mechanisms is important for hazard and risk studies, especially of shallow earthquakes. We implemented a novel, probabilistic full-waveform moment tensor inversion for the application to shallow micro-earthquakes close to gas fields in North Germany. Due to the probabilistic approach, parameter trade-offs, uncertainties and ambiguities are mapped. The implemented bootstrap method implicitly accounts for modelling errors that may affect every station and phase in a unique way. Furthermore, event locations are provided by the algorithm. Such hypocentres, which are estimated simultaneously with moment tensors, are often less sensitive to uncertainties in crustal structure.

November 20th, 2019 M_L 3.0 Kirchlinteln event (21:32 UTC)

The event and two preceding earthquakes are described in detail in [1]. Figure 1 gives an overview on the best solution. This deviatoric moment tensor corresponds to a slightly oblique normal faulting process with most likely northwest-southeast fault strike and a 78⁰ fault dip towards northeast. The centroid moment magnitude Mw is 2.55 and the best source depth is 4.1 km (Figure 1, left), which is within the reservoir (Wintershall DEA Deutschland AG, pers. comm.). Mean and best solution are nearly identical, indicating statistical stability. Figure 1 (right) compares fault traces (Wintershall DEA Deutschland AG, pers. comm.) with the event locations resulting from three inversion runs comprising different input data types for the S-wave records. With respect to the location given in [1], epicentres are shifted slightly to the west or northwest, respectively. The preferred solution displayed in Figure 1 (middle) corresponds to the turquoise star and cross. From these results, we cannot distinguish if the event occurred on the northern, longer NW-SE striking fault or on the southern, shorter segment. Both the preferred solution and the location by [1] favour the latter. It is interesting that the event occurred in the vicinity of fault intersections. The relatively high CLVD component (up to 50%) as well as the radiation pattern may indicate that the N-S oriented fault slipped simultaneously.
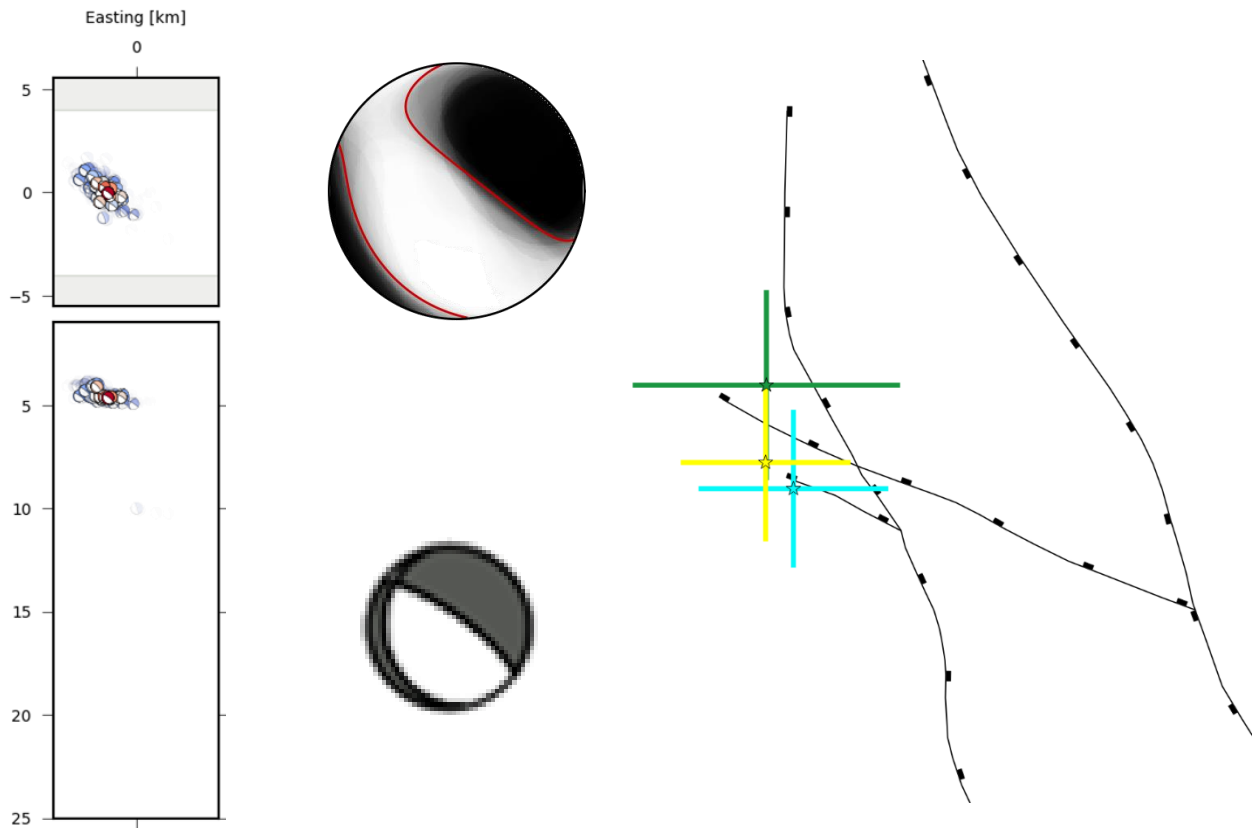
Figure 1: Left: ensemble of event locations with lowest misfit; top middle: best fitting deviatoric moment tensor; bottom middle: double-couple component of the same mechanism; right: fault traces provided by Wintershall DEA Deutschland AG and the event locations resulting from the three best solutions including location uncertainty.

October 1st, 2018 M_L 3.6 Lastrup event (00:28 UTC)

The event, two preceding as well as one subsequent earthquake are described in detail in [2]. gives an overview on the best solution. Since we do not possess information on local faults, we cannot interpret the result in a similar manner as for the Kirchlinteln events. The deviatoric moment tensor corresponds to an oblique thrust faulting process with a fault strike of either ~50⁰ (northeast-southwest) or ~270⁰ (east-west), thus not fitting the larger-scale tectonic structures (, right). The current horizontal maximum stress direction is oriented NW-SE; NW-SE striking faults have been reactivated and new NE-SW striking faults were established (ExxonMobil Production Deutschland GmbH, pers. comm.), which would favour the ~50⁰ striking fault plane, but without information on the vertical and horizontal stress amplitudes does not allow for an interpretation of the stress regime. P-wave first onset polarities fit the favourite solution, though. In addition, [2] mention that the reservoirs are located close to the suture zone, where rock beds of the Lower Saxony tectonic unit partly were thrust on the Pompeckj block. The fault dips ~50⁰, the

interpretation of the dip depends on the fault strike that is more likely.
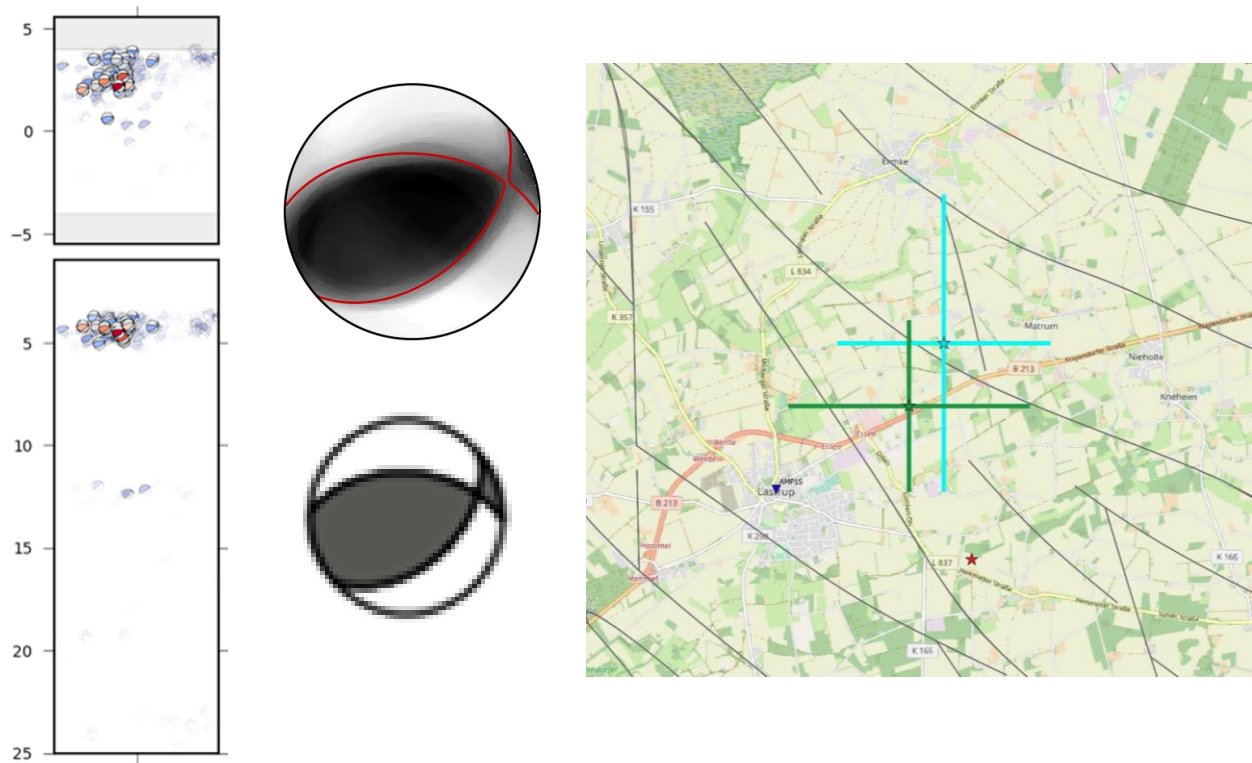
Figure 2: Left: ensemble of event locations with lowest misfit; top middle: best fitting deviatoric moment tensor; bottom middle: double-couple component of the same mechanism; right: regional fault traces at the base of the Zechstein layer provided by LBEG Lower Saxony and the event locations resulting from the two best solutions including location uncertainty.

The centroid moment magnitude Mw is 3.2 for the preferred solution with a best source depth of 4.6 km. Since [2] indicate the depths of gas fields east of Lastrup to be 2200-3750 m, this event potentially occurred beneath and not within the reservoir. Mean and best solution are similar despite a higher CLVD percentage for the mean solution, indicating statistical stability. The best solution represents an almost pure double-couple mechanism and thus, likely a simpler faulting process compared to the Kirchlinteln events involving only a single fault. With respect to the location given in [2], epicentres are shifted slightly to the north or northwest, respectively. The preferred solution displayed in (middle) corresponds to the green star and cross.

Zusammenfassung

Auch wenn Verwerfungen nicht auf geologischen Aufschlüssen sichtbar sind, können die Quellmechanismen von auf diesen Verwerfungen stattfindenden Erdbeben helfen, die Art der Verwerfung zu bestimmen. Zusätzlich stellen Bebenmechanismen einen der wichtigsten Parameter dar, um zwischen natürlichen und induzierten Beben zu unterscheiden sowie die zugrundeliegende Ursache zu erforschen. Informationen über den Bebenmechanismus spielen auch für Studien über die seismische Gefährdung oder Risikoanalysen eine Rolle, speziell im Fall von Flachbeben. In diesem Projekt nutzten wir eine neuartige, probabilistische Momententensorinversion vollständiger Wellenzüge, um Flachbeben mit geringen Magnituden in der Nähe der norddeutschen Gasfelder zu analysieren. Durch den probabilistischen Ansatz werden Parameterkonflikte, Unsicherheiten und Mehrdeutigkeiten abgebildet. Die verwendete Bootstrap-Methodik erlaubt es, Modellierungsfehler implizit zu berücksichtigen, die jede aufzeichnende Station und Wellenphase in unterschiedlichem Maß betreffen können. Zusätzlich liefert der Algorithmus Bebenhypozentren. Solche Hypozentren, die gleichzeitig mit dem Bebenmechanismus abgeschätzt werden, sind häufig weniger von Unsicherheiten in der Kenntnis der Krustenstruktur betroffen.

M_L 3.0 Kirchlinteln Ereignis (20. November 2019, 21:32 UTC)

Das Beben sowie zwei vorhergehende Ereignisse werden im Detail von [1] beschrieben. Abbildung 1 zeigt eine Übersicht über die bestangepassten Lösungen. Der hier gezeigte deviatorische Momententensor entspricht einer leicht schrägen Abschiebung auf einer höchstwahrscheinlich nordwestlich-südöstlich ausgerichteten Verwerfung, die mit 78° nach Nordosten einfällt. Die Momentenmagnitude des Bebenschwerpunkts beträgt Mw 2.55 und die bestangepasste Quelltiefe 4.1 km (Abbildung 1, links), womit das Beben innerhalb der Lagerstätte liegt (Wintershall DEA Deutschland AG, pers. Mitt.). Der bestangepasste und aus dem Ensemble der möglichen Lösungen gemittelte Mechanismus stimmen überein, was auf eine bestehende Stabilität der Inversion hinweist. Abbildung 1 (rechts) vergleicht den Verlauf lokaler Verwerfungen (Wintershall DEA Deutschland AG, pers. Mitt.) mit den Ereignislokationen, die sich aus drei verschiedenen Läufen ergeben und sich durch die Eingabedatentypen unterscheiden, die für den S-Wellenzug verwendet wurden. Verglichen mit der von [1] angegebenen Bebenlokation sind die Epizentren leicht nach Westen bzw. Nordwesten verschoben. Die von uns bevorzugte Lösung, dargestellt in Abbildung 1 (Mitte) entspricht dem türkis eingefärbten Stern bzw. Kreuz. Es kann keine eindeutige Aussage getroffen werden, ob das Beben auf der nördlichen, längeren NW-SE-streichenden Verwerfung stattfand oder auf dem südlicheren, kürzeren Segment. Sowohl die von uns bevorzugte Lösung als auch das von [1] berechnete Epizentrum weisen auf letzteres hin. Interessanterweise trat dieses Ereignis in der Nähe von Knotenpunkten auf. Der relative hohe CLVD-Anteil (bis zu 50%) sowie die Abstrahlcharakteristik könnten bedeuten, dass auf der Nord-Süd orientierten Verwerfung gleichzeitig Bewegungen stattfanden.
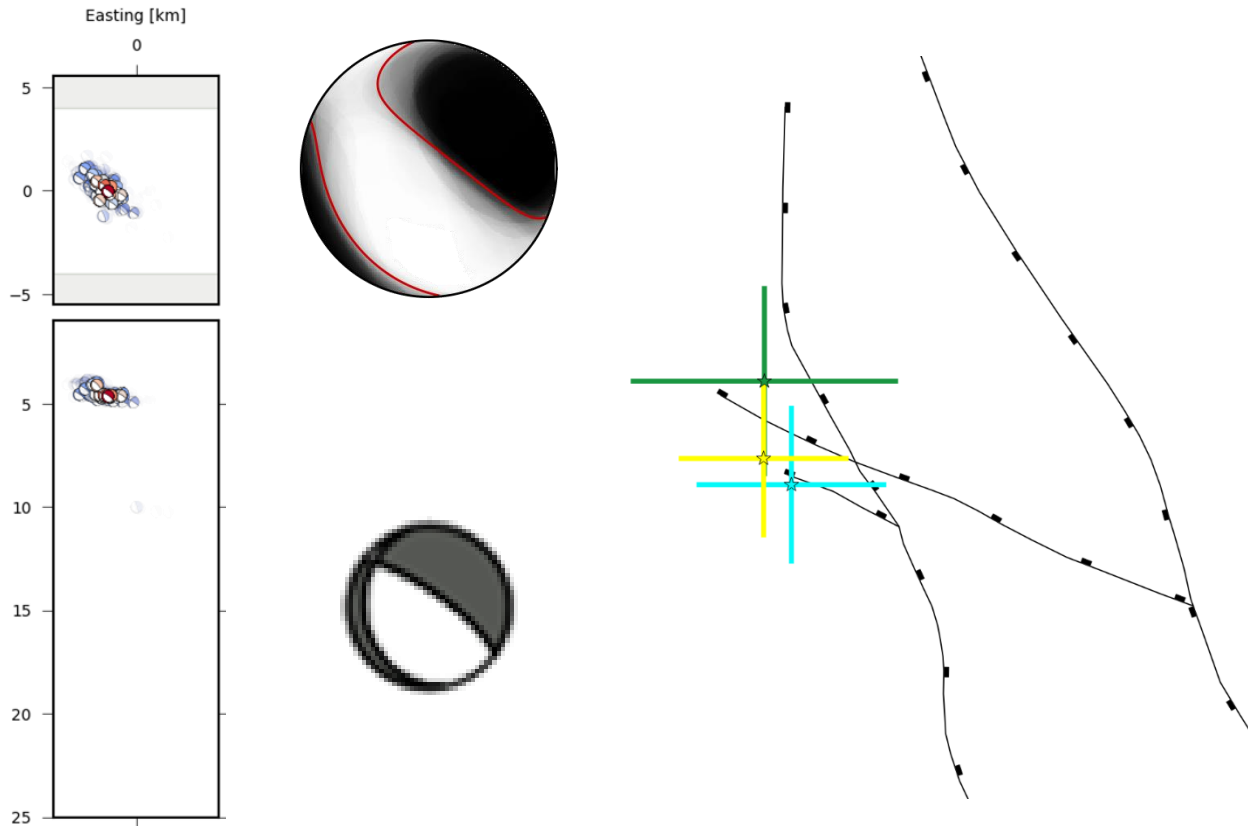
Abbildung 1: Links: Ensemble der Ereignislokationen mit geringstem Anpassungsfehler; Mitte oben: am besten angepasste Lösung für den deviatorischen Momententensor; Mitte unten: zugehörige Herdflächenlösung (double-couple Komponente); rechts: lokale Verwerfungen, von Windershall DEA Deutschland AG zur Verfügung gestellt, sowie Ereignislokationen der drei bestangepassten Lösungen mit Lokalisierungsunsicherheiten.

M_L 3.6 Lastrup Ereignis (01. Oktober 2018, 00:28 UTC)

Das Beben, zwei vorhergehende und ein nachfolgendes Ereignis wurden im Detail von [2] beschrieben. Abbildung 2 zeigt eine Übersicht über die bestangepassten Lösungen. Da wir keine Informationen über lokale Verwerfungen besitzen, können wir das Ergebnis nicht in einer ähnlichen Weise wie für die Kirchlinteln-Beben interpretieren. Der deviatorische Momententensor entspricht einer schrägen Aufschiebung auf einer entweder ~50⁰ (Nordost-Südwest) or ~270⁰ (Ost-West) streichenden Verwerfung und entspricht damit nicht den regionalen Streichrichtungen (Abbildung 2, rechts). Da wir keine Information über das regionale Spannungsfeld besitzen, können wir nicht untersuchen, ob Aufschiebungen in diesem möglich sind, vor allem im Hinblick auf die für die Kirchlinteln-Beben berechneten Abschiebung. Die Polaritäten der auf den nahen Stationen aufgezeichneten P-Welleneinsätze unterstützen die von uns bevorzugte Lösung jedoch. [2] weist außerdem darauf hin, dass die Lagerstätten in dieser Region nahe einer Sutur liegen, an der Festgestein der Niedersächsischen tektonischen Einheit teilweise auf den Pompeckj-Block aufgeschoben wurden. Die Verwerfung fällt mit ~50⁰

5

ein, die Interpretation der Einfallsrichtung hängt von der wahrscheinlicheren Streichrichtung der Verwerfung ab.
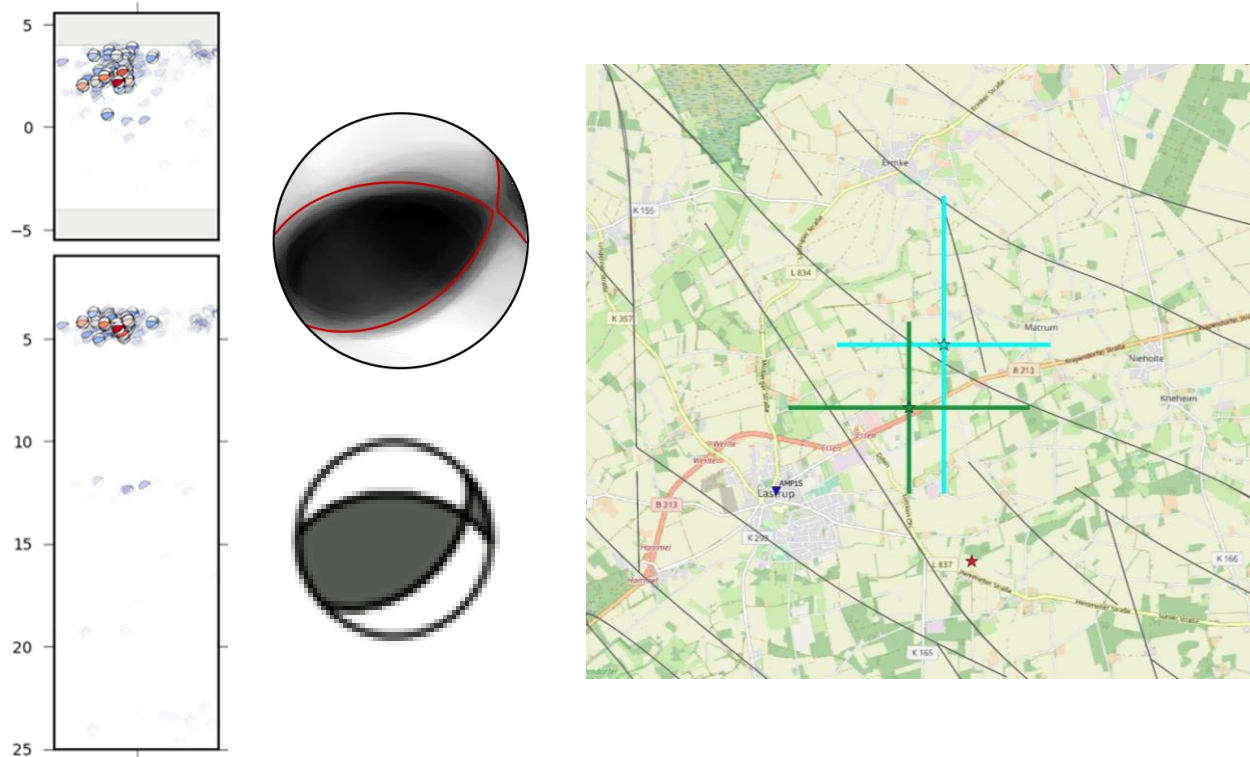

Abbildung 2: Links: Ensemble der Ereignislokationen mit geringstem Anpassungsfehler; Mitte oben: am besten angepasste Lösung für den deviatorischen Momententensor; Mitte unten: zugehörige Herdflächenlösung (double-couple Komponente); rechts: regionale Verwerfungen an der Basis des Zechstein, durch das LBEG Niedersachsen zur Verfügung gestellt, sowie Ereignislokationen der zwei bestangepassten Lösungen mit Lokalisierungsunsicherheiten.

Für die von uns bevorzugte Lösung beträgt die Momentenmagnitude des Bebenschwerpunkts Mw 3.2 und die Quelltiefe 4.6 km. Da [2] die Tiefenlage der Gaslagerstätten östlich von Lastrup mit 2200-3750 m angeben, fand das hier untersuchte Beben möglicherweise unterhalb und nicht in einer Lagerstätte statt. Trotz eines höheren CLVD-Anteils des aus dem Ensemble der möglichen Lösungen gemittelten Mechanismus sind gemittelte und bestangepasste Lösung ähnlich, was wiederum auf eine bestehende Stabilität der Inversion hinweist. Die bestangepasste Lösung lässt sich fast vollständig durch eine Herdflächenlösung beschreiben (entspricht einem reinen double-couple Mechanismus), daher vermuten wir, dass der Bruchprozess einfacher war als die der Kirchlinteln-Ereignisse und die Bewegung nur auf einer einzigen Verwerfung stattfand. Verglichen mit der von [2] angegebenen Bebenlokation sind die Epizentren leicht nach Norden oder Nordwesten verschoben. Die von uns bevorzugte Lösung, dargestellt in Abbildung 2 (Mitte) entspricht dem grün eingefärbten Stern bzw. Kreuz.

1. Motivation

Even if faults are not visible on geological outcrops, source mechanisms of earthquakes occurring on those faults may distinguish between different types of faulting. Moreover, the source mechanism of seismic events is one of the most important parameters to discriminate between natural and induced earthquakes and helps to understand the underlying cause. In addition, information on source mechanisms is important for hazard and risk studies, especially of shallow earthquakes. We implemented a novel, probabilistic full-waveform moment tensor inversion ("grond", [3]) for the application to shallow micro-earthquakes close to gas fields in North Germany (for details, see 3). The method was previously applied successfully to investigate induced events in the Groningen gas field in the Netherlands ([4]; [5]). Due to the probabilistic approach, parameter trade-offs, uncertainties and ambiguities are mapped. The implemented bootstrap method implicitly accounts for modelling errors that may affect every station and phase in a unique way. Furthermore, event locations are provided by the algorithm. Such hypocentres, which are estimated simultaneously with moment tensors, are often less sensitive to uncertainties in crustal structure.

2. Data

In addition to the stations of the BVEG network (http://www.seis-info.de/), we included nearby sensors of the GRSN (German Regional Seismic Network; https://www.seismologie.bgr.de/doi/grsn/) and GE (GEOFON; https://geofon.gfz-potsdam.de/doi/network/GE) networks into our study. Since sensor types differ between and even within networks, we carefully evaluated station quality using the AutoStatsQ toolbox ([6]) and additional methods. Exemplarily, Figure 3 shows the variety of instruments installed in the region of the November 20th, 2019 Kirchlinteln events. Figure 4 demonstrates waveforms recorded at less than 25 km epicentral distance to the October 1st, 2018 M_L 3.6 Lastrup event (00:28 UTC), while Figure 5 represents station whose records were employed for its inversion.

For the analysis of the latter event, we included waveforms recorded on selected stations of the Dutch seismological network in order to close the azimuthal gap towards the West. For all events analysed, it did not seem to be advantageous to employ surface waves in the analysis; hence, we inverted seismic traces for time windows fitted to the P- and S-wave arrivals. Time windows were chosen according to manually picked onset times.
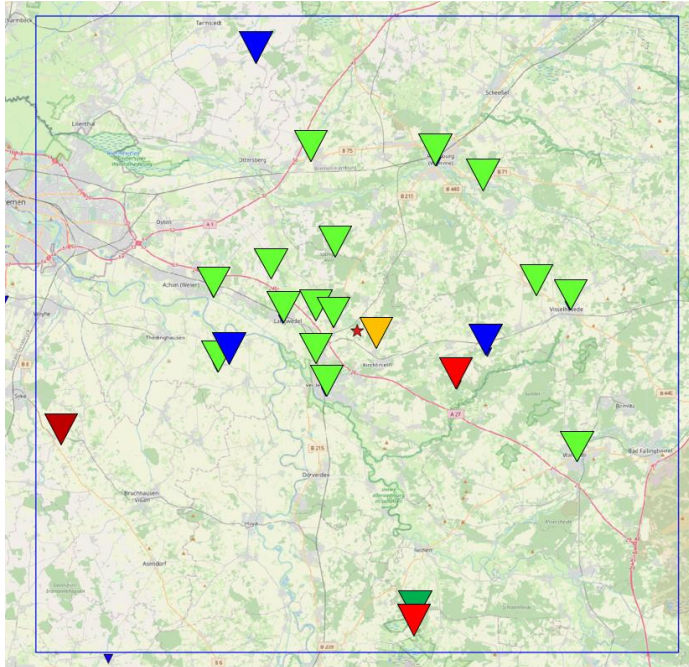
Figure 3: Types of instruments installed in the area of the November 20th, 2019 Kirchlinteln events. The red star marks the location of the M_L 3.0 event at 21:32 UTM. The blue rectangle measures 30 x 30 km².
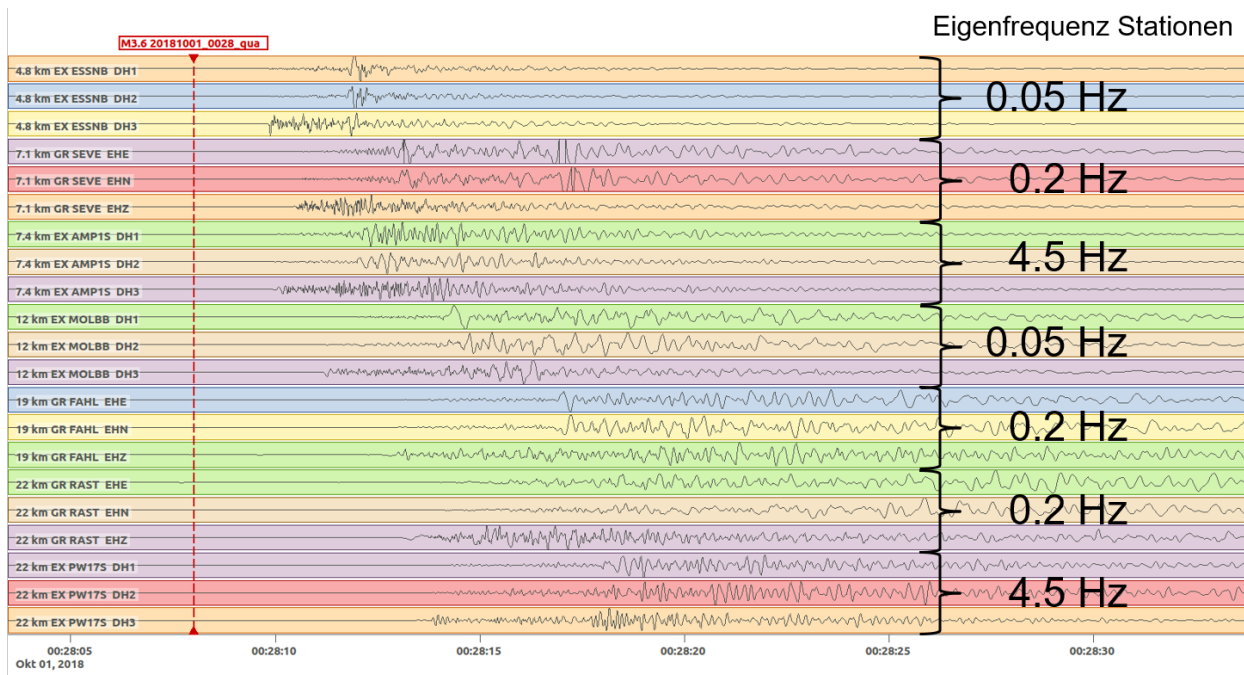
*Figure 4: Example seismograms showing the October 1st, 2018 ML 3.6 Lastrup event (00:28 UTC). Stations including network, component and epicentral distance employing the locations of [2] indicated to the left. The red dotted vertical line gives the event's origin time. Eigenfrequency of recording stations shown to the right. S-phases clipped on horizontal components of stations ESSNB (BVEG network) as well as SEVE (GRSN).*
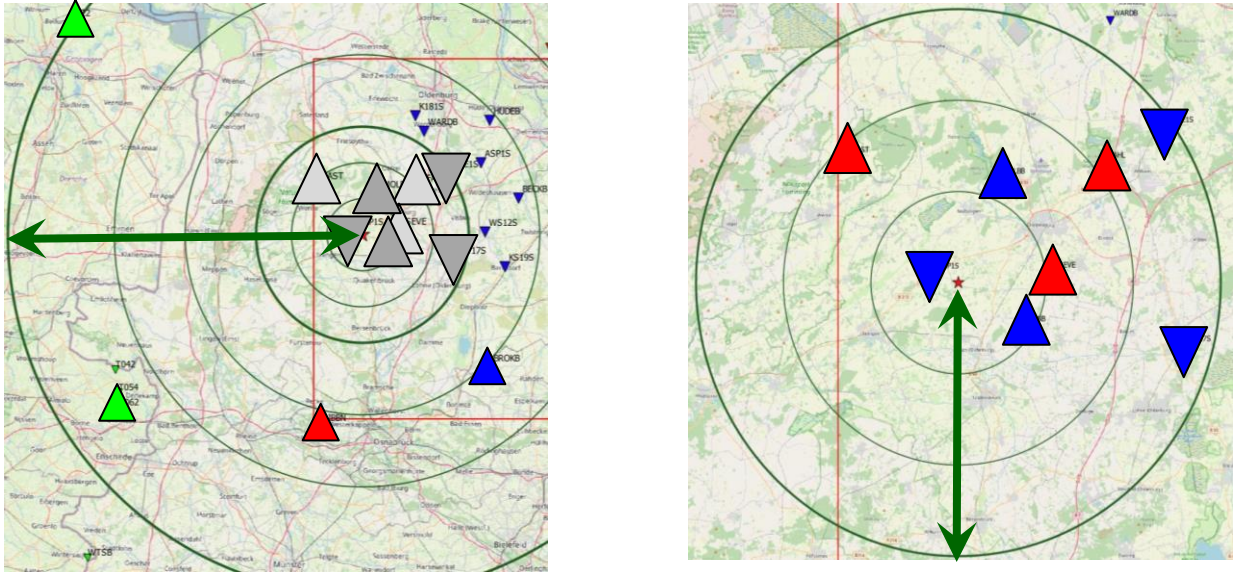
Figure 5: Stations employed for the inversion of the October 1st, 2018 ML 3.6 Lastrup event (00:28 UTC); red triangles: GE/GR network broadband stations, blue triangles: EX network broadband stations, inverted triangles: EX network short period stations, green triangles: NL network mid-period stations; left: epicentral distances up to 30 km as marked by the green arrow; right: epicentral distances up to 100 km as marked by the green arrow.

In order to stabilise the inversion of the Lastrup event that is located at the western margin of the BVEG network, we took into account stations of the GE, GR and EX network up to 30 km epicentral distance but complemented these to the south with broadband stations IBBN (GE network) and BROKB (EX network). Further, we included records from stations of the Dutch network run by KNMI to close the azimuthal gap towards the west. For this purpose and after a careful quality control, we chose borehole stations G223 and T062. The incorporation of the Dutch broadband station WTSB, on the other hand, did not bring an additional advantage.

Furthermore, we performed detailed tests of input data types and inversion parameters to derive rules of good practice. Details of the station quality analysis and further tests can be found in section 5.

3. Moment tensor inversion methodology

Inverting full waveforms instead of P-wave polarities increases the information content (taking into account multiple amplitudes, not only for the P-, but also for the S-wave). P-wave polarities, especially for emerging onsets and low signal-to-noise ratio records, can be difficult to identify. Ambiguities are not represented in the final solution, which is a problem especially for low magnitude events or patchy station coverage. The dependence of the polarity on the source radiation angle needs to be accounted for manually and its

relation to the velocity model often is not sufficiently analysed. A full moment tensor inversion automatically accounts for these circumstances and always delivers the optimum solution; the algorithm described below searches for an optimum solution for both source mechanism and event location simultaneously. The main advantage of the probabilistic inversion is that parameter errors, uncertainties and trade-offs can be taken into account. The interpretation of the deviatoric instead of limiting the inversion to a double couple solution as for the focal mechanism inversion may carry additional information.

We implemented the inversion using the Grond framework ([3]), an open-source Python software package for probabilistic earthquake source inversion based on the Pyrocko package ([7]). Among other events, the methodology was previously applied to events in the Groningen gas field, the Netherlands ([4]; [5]). The latter paper describes the methodology in more detail; therefore, it will only be summarised shortly in the following. We computed source model estimates and uncertainties by employing a bootstrap-based probabilistic joint inversion. The optimization routine offers a flexible design of objective functions, explores the full model space, and maps model parameter trade-offs. Forward modelling is accelerated by the use of precomputed Green's function databases, which are handled by the related Python Pyrocko-GF software library ([8]). For forward modelling of regional seismological data, the incorporated orthonormal propagator method QSEIS ([9]) is well suited. The pre-processing of waveforms involves the removal of instrument responses, frequency band-limited conversion to displacement, and extraction of desired phases by tapering. The misfit between observed and synthetic data is represented by an objective function, the global minimum of which is searched during the optimization process. Input data, weights, norm, and error treatment influence the shape of the objective function. We systematically explored different combinations of waveform processing and misfit functions in either time or frequency domain. Misfits are normalised in groups to enable relative weighting of individual waveform misfits. For optimization, the Bayesian bootstrap optimization algorithm ([3]) is employed. Multiple objective functions are explored in parallel as individual bootstrap chains, which allows for a probabilistic interpretation of the result ensemble. During each iteration, an individual misfit is computed for each bootstrap chain. Each bootstrap chain differs from the others by an additional random weight factor. From the combination of results from all bootstrap chains' high-score lists, the best and mean solutions can be retrieved. A comparison between best and mean solution delivers acts as indicator for the stability of the inversion. The fuzzy moment tensor plots indicate ambiguities in the solution.

For both Kirchlinteln and Lastrup events, already synthetic studies showed that stations from the different networks should be combined as well as different input data types. Especially the merging of different kinds of information (e.g. time traces, amplitude spectra, cross-correlation traces) is not standard, but can be accomplished without

difficulty by the Grond algorithm. During the inversion, different combinations of stations velocity models, input data types and inversion parameters were tested. The modus operandi will be described in detail in an upcoming publication.

As input data types, we tested time traces, amplitude spectra and cross-correlation traces of both P- and S-wavetrains in various combinations. Arrival time information was best used to define the P- and S-wave time windows employed in the inversion. Although it is beneficial to include records from as many high-quality stations as possible, it transpired as favourable to include only cross-correlation traces from stations with erroneous sensitivity in the stationXML file, instead of the absolute amplitude information. In addition, while it emerged as advantageous to combine different data types for each wave class, results deteriorated when including P-wave spectra.

4. Inversion results

November 20th, 2019 M_L 3.0 Kirchlinteln event (21:32 UTC)

The event and two preceding earthquakes are described in detail in [1]. Figure 6 gives an overview on the best solution. This deviatoric moment tensor corresponds to a slightly oblique normal faulting process with most likely northwest-southeast fault strike and a 78º fault dip towards northeast. The centroid moment magnitude Mw is 2.55 and the best source depth is 4.1 km (Figure 6, left), which is within the reservoir (Wintershall DEA Deutschland AG, pers. comm.). Mean and best solution are nearly identical, indicating statistical stability. Figure 6 (right) compares fault traces (Wintershall DEA Deutschland AG, pers. comm.) with the event locations resulting from three inversion runs comprising different input data types for the S-wave records. With respect to the location given in [1], epicentres are shifted slightly to the west or northwest, respectively. The preferred solution displayed in Figure 6 (middle) corresponds to the turquoise star and cross. From these results, we cannot distinguish if the event occurred on the northern, longer NW-SE striking fault or on the southern, shorter segment. Both the preferred solution and the location by [1] favour the latter. It is interesting that the event occurred in the vicinity of fault intersections. The relatively high CLVD component (up to 50%) as well as the radiation pattern may indicate that the N-S oriented fault slipped simultaneously.
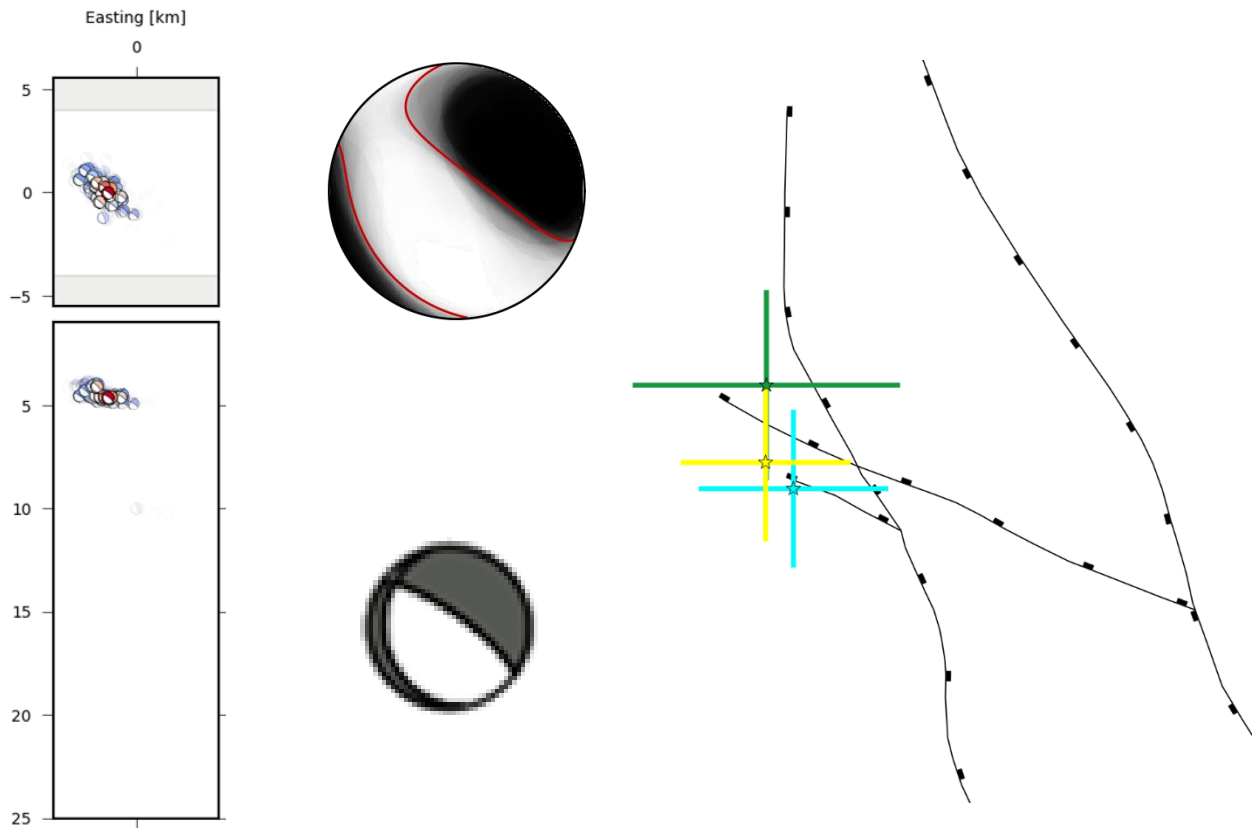
Figure 6: Left: ensemble of event locations with lowest misfit; top middle: best fitting deviatoric moment tensor; bottom middle: double-couple component of the same mechanism; right: fault traces provided by Wintershall DEA Deutschland AG and the event locations resulting from the three best solutions including location uncertainty.

Remaining November 20th, 2019 Kirchlinteln events

The preceding event at 17:28 UTC with a similar magnitude turned out to be more difficult to invert, although waveforms, when filtered in the low frequency range (0.01 – 2 Hz for broadband, 0.5 – 2 Hz for short period stations), are similar (see section 5). If records from short-period stations are included, the solutions are very unstable. The result may be enhanced by employing only broadband stations, but neither mechanism nor event locations are well-defined. The intermediate event at 19:52 UTC, although only recorded at five stations due to its lower magnitude, shows a mechanism similar to the 21:32 UTC event but with higher uncertainty and a less well-defined event location (Figure 7).

12
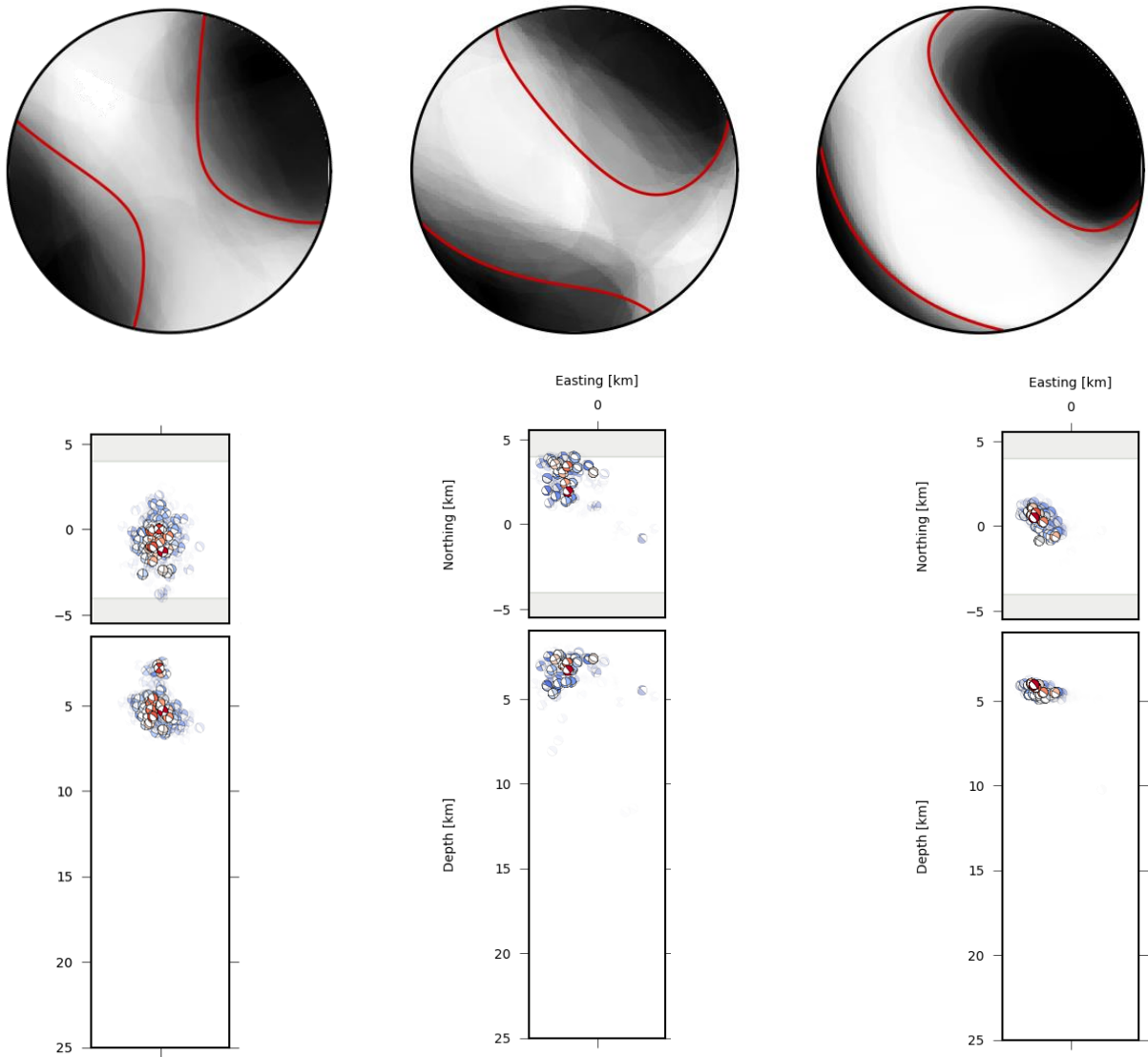
Figure 7: Results for ensemble of lowest misfit solutions. Top: stacked radiation pattern, global best solution indicated in red, if variability of the ensemble solutions is small, the fuzzy plot has clearly separated black and white fields; bottom: event locations, symbols show best double-couple mechanisms, colours indicated misfit (blue – high, red – low).

The fuzziness of the resulting moment tensor plot for the event at 17:28 UTC indicates a large variability between, i.e. instability of, solutions. The double couple mechanism (not shown here) shows strike-slip instead of normal faulting as expected, which may be caused by residual instability in the inversion process. Since just broadband stations are considered, due to their careful installations, partly in boreholes, the signal-noise-ratio should not differ too much despite the different timing of events. Interestingly, the first event seems to be located closer to the epicentre given by [1] and thus, more to the south closer to the intersection with the N-S striking fault. Our hypothesis is that the first event is more difficult to invert since the faulting process was more complex. Since it in addition

13

possesses a higher magnitude, we believe that two faults have moved simultaneously during the 17:28 UTC event.

If we accept the local magnitudes computed by [1], according to Båth's law ([10]), the magnitude difference between first and third event is too small for the latter to represent a mere aftershock, since aftershock magnitudes are expected to be lower than $M_L^{(aftershock)} < M_L^{(main)}$ -1.2 = 1.8, which is a further indication of a more complex fracture process.

In addition to inverting for a deviatoric mechanism, we tested a full moment tensor inversion, but this results in both unstable CLVD and isotropic components, such that we do not recommend the approach. This is most likely due to an insufficient coverage of the region by high-quality stations (e.g. broadband or borehole stations).

October 1st, 2018 M_L 3.6 Lastrup event (00:28 UTC)

The event, two preceding as well as one subsequent earthquake are described in detail in [2]. Figure 8 gives an overview on the best solution. Since we do not possess information on local faults, we cannot interpret the result in a similar manner as for the Kirchlinteln events. The deviatoric moment tensor corresponds to an oblique thrust faulting process with a fault strike of either ~50⁰ (northeast-southwest) or ~270⁰ (east-west), thus not fitting the larger-scale tectonic structures (Figure 8, right). The current horizontal maximum stress direction is oriented NW-SE; NW-SE striking faults have been reactivated and new NE-SW striking faults were established (ExxonMobil Production Deutschland GmbH, pers. comm.), which would favour the ~50⁰ striking fault plane, but without information on the vertical and horizontal stress amplitudes does not allow for an interpretation of the stress regime. P-wave first onset polarities fit the favourite solution. In addition, [2] mention that the reservoirs are located close to the suture zone, where rock beds of the Lower Saxony tectonic unit partly were thrust on the Pompeckj block.

The fault dips ~50⁰, the interpretation of the dip depends on the fault strike that is more likely.
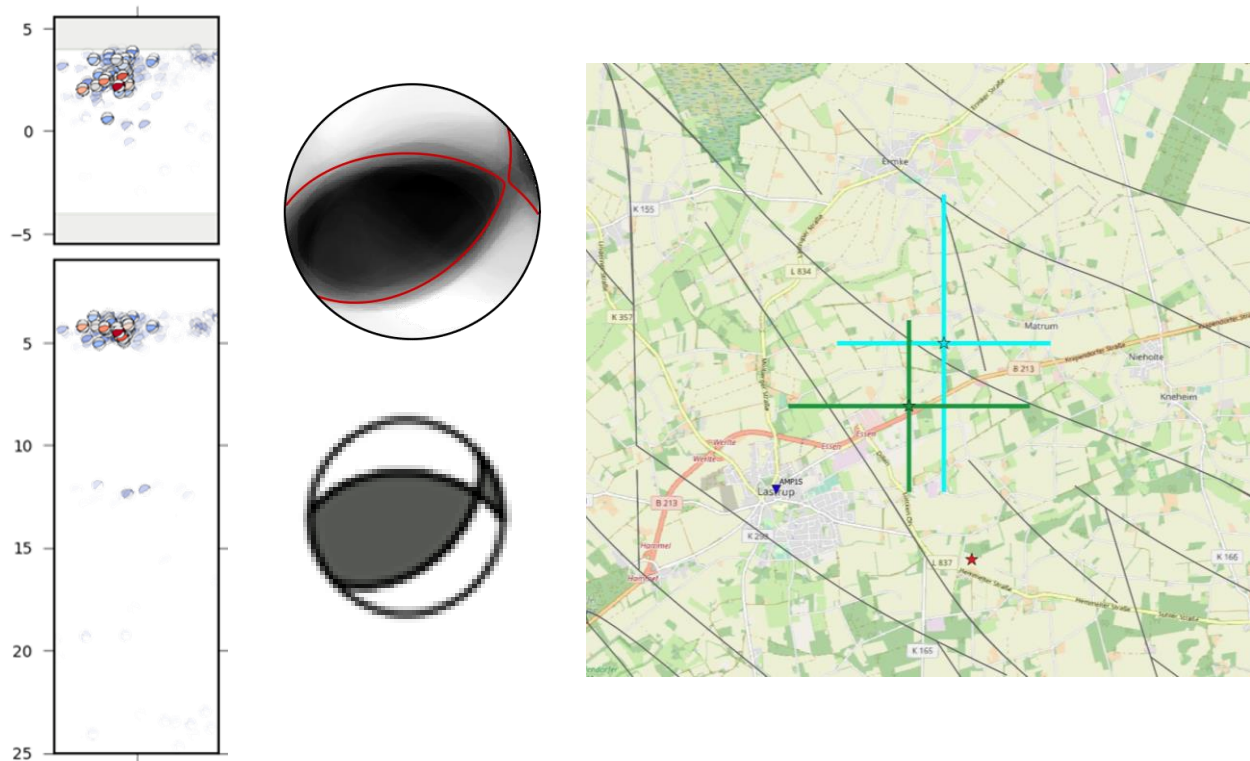

Figure 8: Left: ensemble of event locations with lowest misfit; top middle: best fitting deviatoric moment tensor; bottom middle: double-couple component of the same mechanism; right: regional fault traces at the base of the Zechstein layer provided by LBEG Lower Saxony and the event locations resulting from the two best solutions including location uncertainty.

The centroid moment magnitude Mw is 3.2 for the preferred solution with a best source depth of 4.6 km. Since [2] indicate the depths of gas fields east of Lastrup to be 2200-3750 m, this event potentially occurred beneath and not within the reservoir. Mean and best solution are similar despite a higher CLVD percentage for the mean solution, indicating statistical stability. The best solution represents an almost pure double-couple mechanism and thus, likely a simpler faulting process compared to the Kirchlinteln events involving only a single fault. With respect to the location given in [2], epicentres are shifted slightly to the north or northwest, respectively. The preferred solution displayed in Figure 8 (middle) corresponds to the green star and cross.

September and October 2018 Lastrup events
The remaining three events that occurred on the 28.09.2018 (16:21 UTC), 01.10.2018 (0:26 UTC) and 17.10.2018 (23:56 UTC) were not inverted during the course of this project. However, since already the inversion of the largest magnitude event was difficult due to the epicentre being located at the margin of the BVEG network, such that station records from the Netherlands Meteorological Institute (KNMI) had to be included in the analysis, most likely the second and third event, possessing magnitudes of M_L 2.1 and

2.5, respectively, will not result in a satisfying solution. The event on the 01.10.2018 at 0:26 UTC occurred only two minutes before the event for which a moment tensor was computed and thus most likely represents a foreshock, potentially with a very similar mechanism. It would be interesting to analyse the event that took place on the 28.09.2019, though, in order to infer if it occurred on the same fault.

5. Additional studies

Station quality

For displacement-based analysis methods as moment tensor inversion, applying the instrument correction to data is essential. Erroneous amplitude information needs to be recognised and corrected or dismissed. To ensure a sufficient data quality to enable the moment tensor inversion, the quality of the station metadata as noted in the stationXML files was analysed in-depth. Detailed results are available in [11] for the GRSN stations as well as in [12] for the BVEG network stations, such that we only provide a short summary here. For both networks, the metadata had to be corrected manually, e.g. due to errors in station elevation and depth (GRSN), missing specifications (BVEG) or a mismatch in channel naming between data, file names and metadata (BVEG network). Further, a few stations were detected in both networks for which the instrument sensitivity value given in the metadata is inconsistent with the sensitivity computed from the complete response.
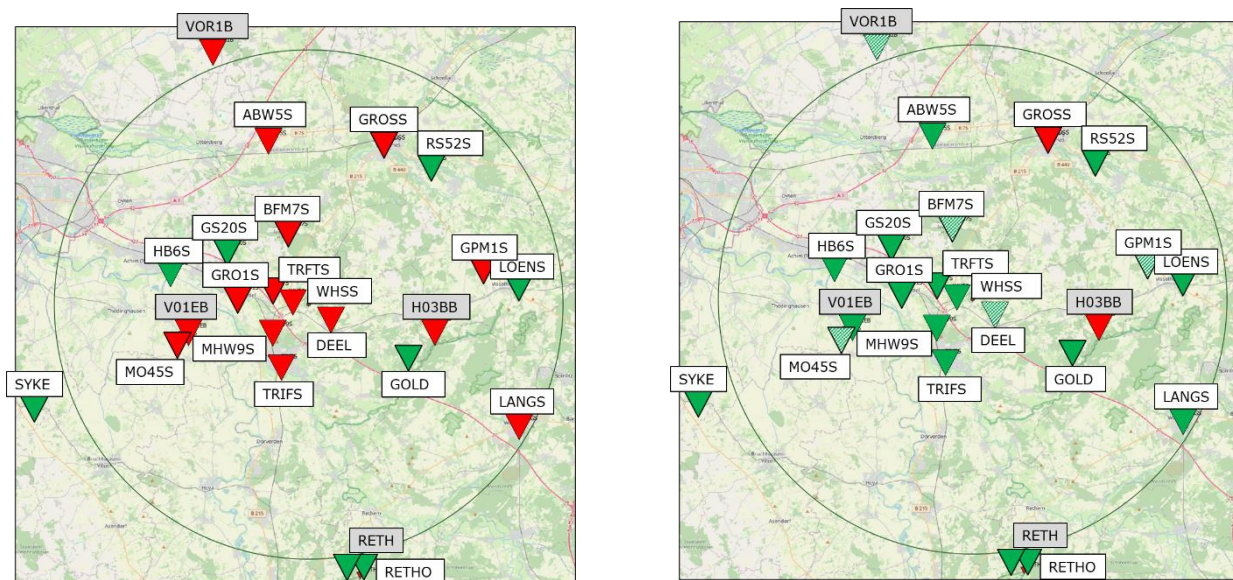
Figure 9: Lowest (left) and highest (right) number of stations employed for inversion of Kirchlinteln events; red triangle: station records omitted, green triangle: station records used, green-striped triangle: records only adopted as cross-correlation traces omitting amplitude information

For the GRSN network, several stations were identified with errors in the horizontal component orientations. For other stations, the results of the orientation analysis were

ambiguous. One station seems to feature a gain that is too low. For the short-period stations of the BVEG network, an analysis of the orientation of horizontal components employing records of teleseismic events is not possible due to their low frequency content. Results derived from alternative methods are mostly inconclusive, while the analysis of the gain was inconspicuous. The analysis of the polarity of vertical components did not reveal any errors for both networks. In the time period of the November 20th, 2019 Kirchlinteln events, station GROSS in the BVEG network seems to have a problem with time registration. We tested different station combinations (Figure 9), considering uncertainties in orientation analysis and sensitivity, problems while adapting the record amplitudes during the inversion process, which may be caused by site effects, and results from the H/V study. The most advantageous station combination transpired as including as many stations as possible, excluding only clearly misfunctioning stations GROSS and H03BB (BVEG network), but employing only cross-correlation traces from stations with erroneous sensitivity indicated in the stationXML file, thus disregarding the amplitudes.

Usable frequency range

The smaller the earthquake magnitude, the higher the dominant frequency content of the recorded signals. At the same time, inverting data at higher frequencies requires knowledge on smaller-scale structures in the subsurface, and thus, inverting the data at low frequencies is desirable. The frequency range available for moment tensor inversion is limited on the upper end by the available sampling frequency, which usually is not critical, as well as the instrument characteristics on the lower end. The instrument's eigenfrequency is a stable indicator of a safe lower frequency limit, however, if the recording stations are of the short period type, the dominant frequency content of the waveforms may be lower, effectively impeding the use of data recorded on such instruments. Because the DMTS3D instruments employed in the BVEG network possess an eigenfrequency of 4.5 Hz, while a visual analysis of waveforms revealed the most suitable frequency range for inversion to be 0.5 to 2 Hz, we performed an analysis of the power spectral density of ambient seismic noise recorded on all stations within 24 hours on the day before the Kirchlinteln event with the result that data recorded on instruments of type DMT S3D will be inverted in the frequency range of 1.7 to 5 Hz, while data registered on all other instruments will be inverted in the range of 0.5 to 2 Hz (Figure 10).
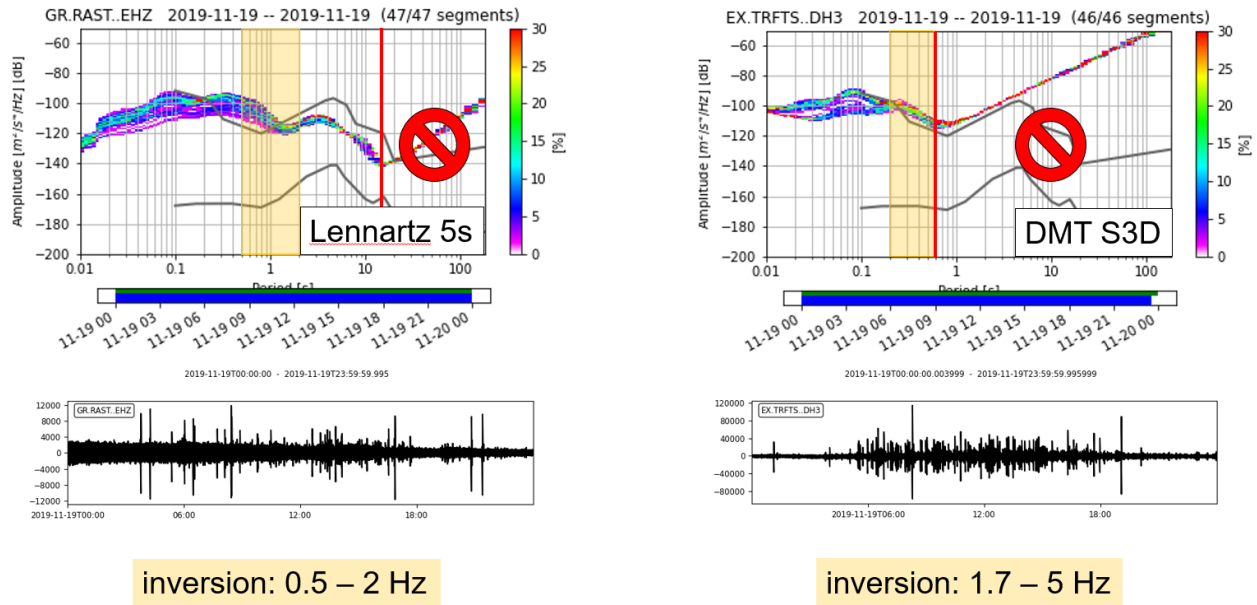
Figure 10: Power spectral density (PSD, top) for stations GR.RAST of type Lennartz 5s (left) and EX.TRFTS of type DMT S3D (right). The PSD has been computed for 47 and 46 time windows marked by different colours, respectively recorded on the 19th November 2019 (full trace displayed at the bottom). Top: periods higher than indicated by the red line should not be employed in the moment tensor inversion. Orange rectangle shows frequency range selected for the respective instrument type (0.5 to 2 Hz for the Lennartz 5s, 1.7 to 5 Hz for the DMT S3D sensor). Grey lines mark the low and high new noise models by [13].

Velocity models

Due to the complexities in the subsurface structure including salt pillows and domes, we refrained from employing a regional velocity model and instead constructed local velocity models by extracting 1-D models from a full 3-D model ([14]). However, this velocity model only reaches a depth of 5~km and seismic velocities can be trusted only up ~4 km depth (pers. comm., industry partners). In order to model seismic waveforms at larger epicentral distances, the velocity model was continued to below Moho depth using interpreted refraction seismic profiles measured in north Germany ([15]) and reprocessed by J. Mechie (GFZ, pers. comm.). For the Lastrup events, three velocity models were tested, a regional model extracted from the CRUST2.0 model ("qlb"; [16]), a local extracted at the epicentre ("qn") and a model averaged from 443 1-D profiles extracted within 12 km epicentral distance ("q2s"). The inversion results using the locally averaged model were most satisfying. Only for the stations with epicentral distances larger than 30 km, the CRUST2.0 velocity model was employed during the inversion ("qlb").
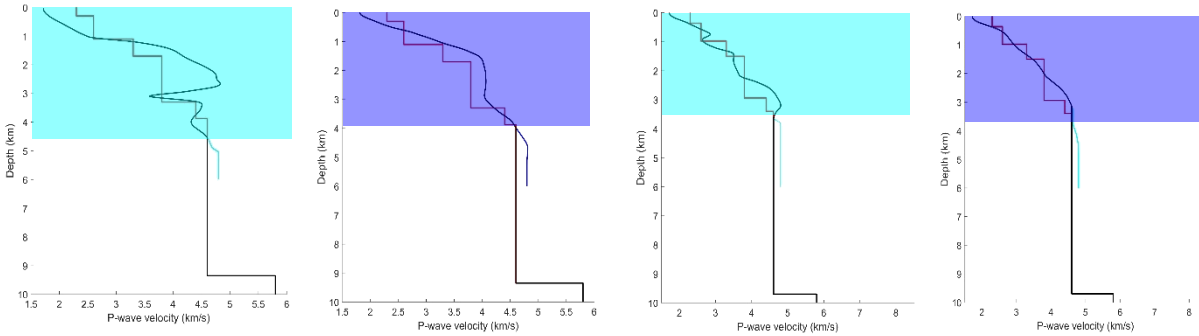
Figure 11: 1D-velocity models employed in the inversion, the coloured area corresponds to the profile extracted from the 3D model ([14]). From left to right: model extracted at event location of Kirchlinteln event, model averaged around location of Kirchlinteln event, model extracted at location of Lastrup event, model averaged around location of Lastrup event.
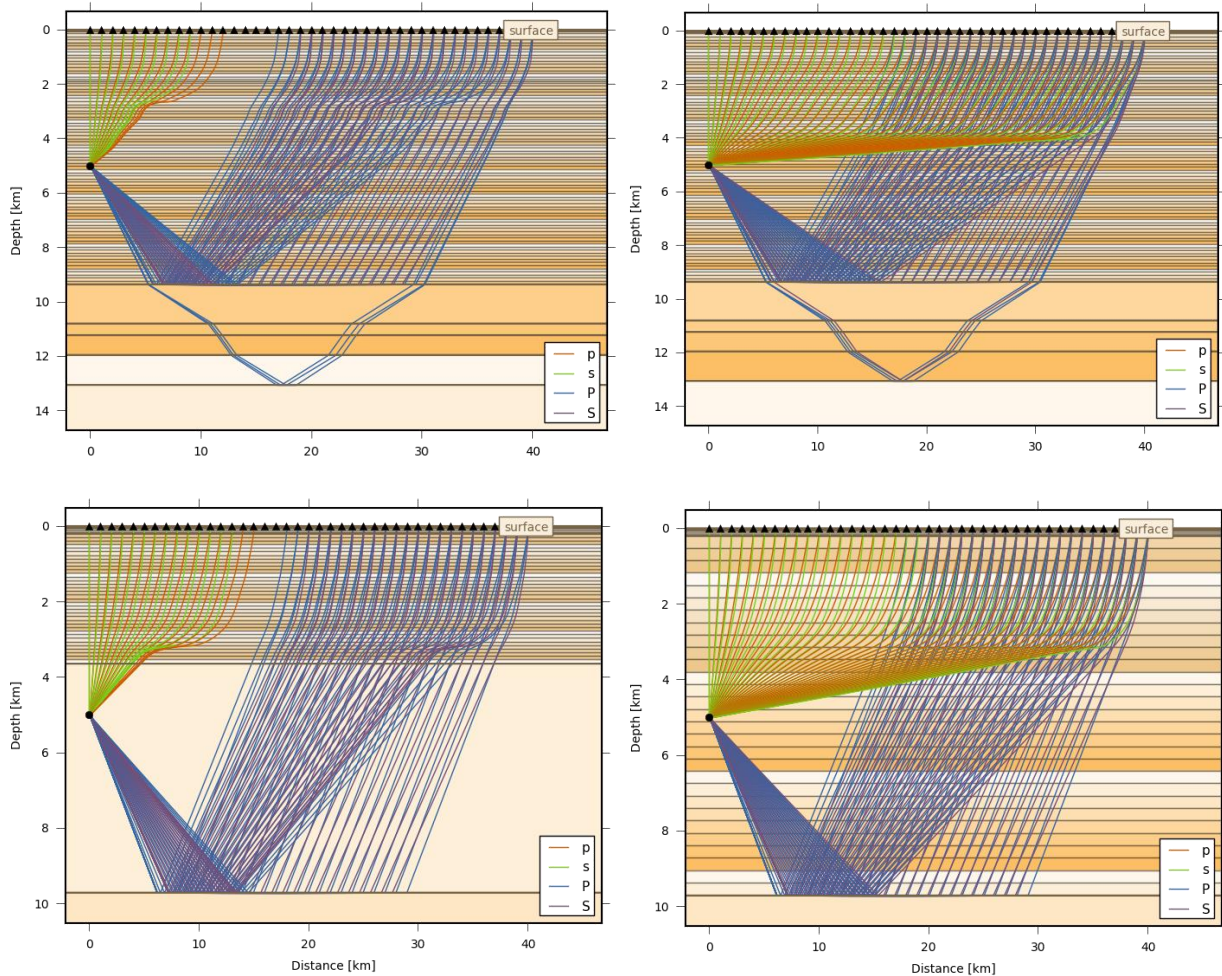

Figure 12: Comparison of ray tracing in different velocity models for a source depth of 5 km and source-receiver distances up to 40 km. Top row: velocity models for Kirchlinteln region, bottom row: velocity models for Lastrup region. Left column: velocity model extracted at event location, right column: velocity model averaged from suite of 1D models.

For the Kirchlinteln events, we likewise compared results for a local model extracted at the epicentre ("lw") and a model averaged from 448 1-D profiles extracted within 12.5 km epicentral distance ("lw2") but supplemented those by four additional profiles gained by grouping 1D models extracted at station locations. The profile extracted at the event location seems to best represent stations located to the east, while profiles "sg1" and "sg2" correspond to stations located to the west and north, respectively. 1D models extracted at stations TRIFS (BVEG network) and GOLD (GRSN) network do not fit any of the groups. In order to identify the best inversion parameters, we assigned different velocity models to stations. Figures Figure 11 and Figure 12 display the key velocity models and examples of ray tracing based on these models.

H/V

The analysis of ambient vibration fields is a valuable tool for characterising the shallow subsurface properties (e.g., [17]; [18]). The single-station H/V analysis allows the estimation of the fundamental resonance period of low impedance sediment layers overlaying higher impedance materials (e.g., [19]). Although the methodology was developed to perform microzonation surveys for earthquake hazard (e.g., [20]), it transformed into a geophysical exploration tool to assess soil and sedimentary thickness, ranging from tens of metres to more than 1,000 m (e.g., [21]).

In this study, we are mainly interested in obtaining a qualitative estimate of potential site effects at station locations, since such site effects could represent an obstacle for the moment tensor inversion, because they are not represented in the velocity model. Figure 13 shows examples of H/V spectra computed from a 24-hour time trace recorded on the day before the Kirchlinteln event.
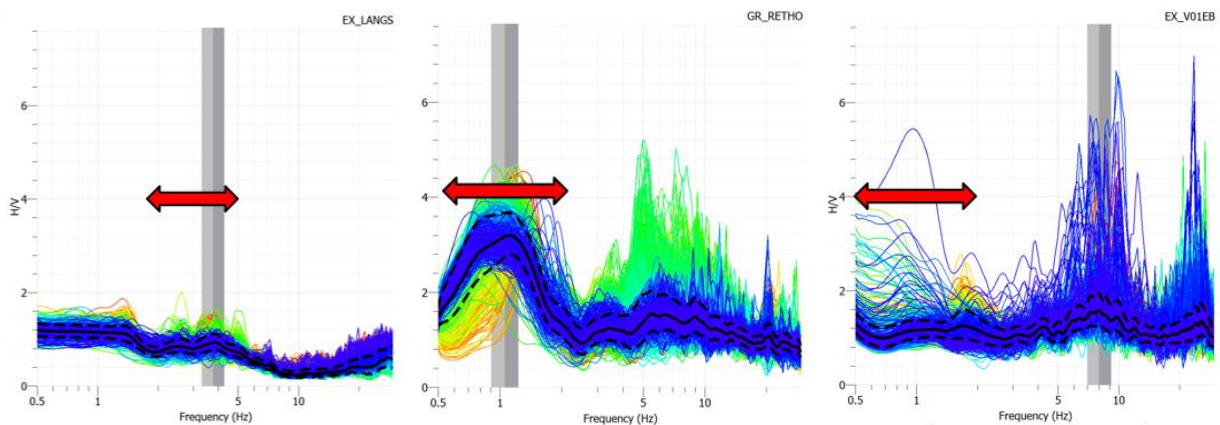

Figure 13: Exemplary H/V spectra. Left: station EX.LANGS, middle: station GR.RETHO, right: station EX.V01EB. Data were filtered in the frequency range 0.5 to 30 Hz and spectra were computed for time windows of 2 mins length and are coloured according to time. Red arrow denotes frequency range used for inversion of data recorded on this specific station.

Most stations in the region of Kirchlinteln show no or only small amplitude peaks (left), while a few feature larger amplitude peaks indicating a velocity contrast in the subsurface that may lead to amplitude amplification (middle), while at some stations, spectra are unstable in time, indicating a temporally varying level of human-made noise close to the station (right). This behaviour is extreme for station EX.H03BB and is also visible on the recorded time trace. If present, the frequency at which the peak appears in the spectrum indicates the depth to the velocity contrast (depending on the shear wave velocity in the overlaying medium). Figure 14 presents an overview of measured peak amplitudes and frequencies for the stations in the BVEG and partly GRSN networks.
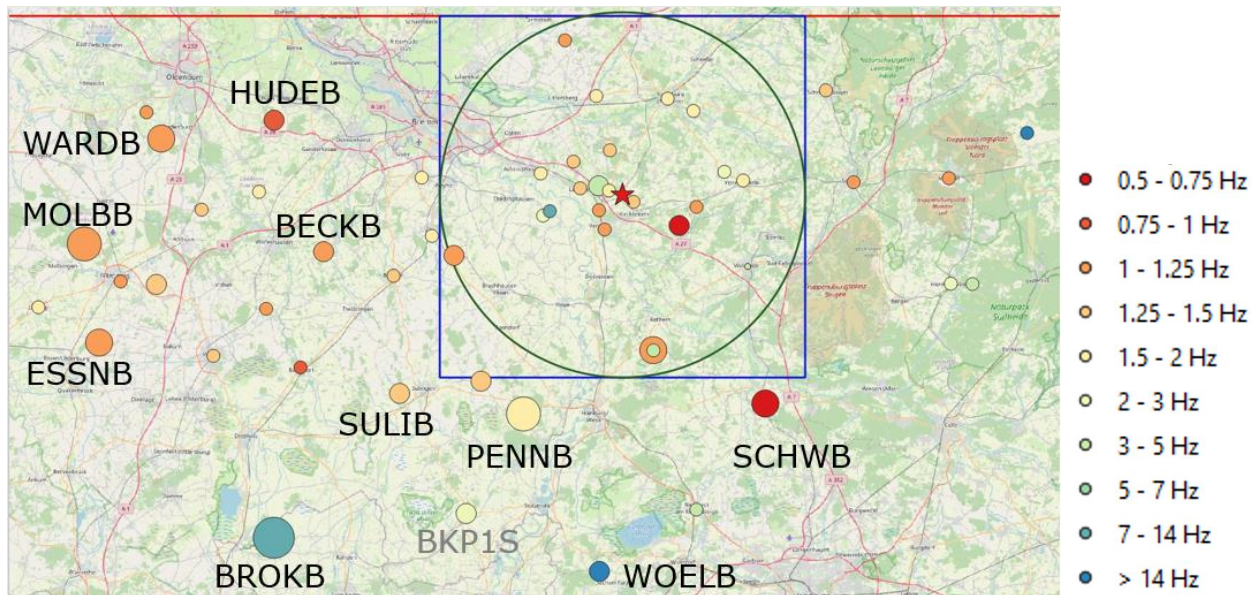

Figure 14: H/V peak frequencies for stations of the BVEG and partly GRSN networks. Circle sizes are proportional to peak amplitudes, while circle colour indicates the peak frequency.

Curiously, stations of the BVEG network featuring high peak amplitudes are almost exclusively installed in boreholes and in general, GR stations, although installed at the surface, show higher peak amplitudes than neighbouring BVEG short period stations. [22] compared accelerometer records between stations installed in buildings and on the free field and concluded that waveform records in buildings significantly underestimated the ground movement by 40-90% for frequencies larger than 8 Hz. This deviation was especially significant for stations installed in large buildings. Since the BVEG short period stations are installed in buildings as well, such a general trend in H/V peak amplitudes may indicate an influence of these buildings on the waveform records. Due to the goal of these measurements being the estimation of the influence of shaking on buildings, this may not present a problem; however, the question remains how well ground shaking in smaller (residential) houses may be estimated from ground shaking records registered in large buildings. For the aim of our study, we assumed for now that the short period station records are not damped.

Comparison of waveforms for Kirchlinteln

If waveforms recorded during the three events on November 20th, 2019, are compared in a low frequency range, they appear to be similar (

). Between first and third events, waveforms are shifted with respect to each other, which can be explained by a slightly different event location or an effect of rupture directivity. Seismic traces for the second event possess a lower signal-to-noise ratio due to the smaller event magnitude, but otherwise are almost identical to the records of the third event, implying an identical mechanism and event location.

Directivity

A rupture directivity analysis employing the empirical Green's function (EGF) methodology ([23]) was performed additionally for the 20th November 2019 17:28 UTC Kirchlinteln earthquake by J. A. López Comino. Unfortunately, only few stations recorded the smaller magnitude event at 19:52 UTC employed as EGF, namely stations BFM7S, MHW9S, TRFTS, V01EB (BVEG network) as well as DEEL, RETH and RETHO (GR network) resulting in large uncertainties of the result. Further, as stated above, the faulting mechanism of the first event in the series may have been more complex and thus, its mechanism not sufficiently similar to comply with the methodology's requirements. The results show, however, that a bilateral rupture fits the apparent source duration better than a unilateral rupture. The most likely fault strike is between 305º ≤ strike ≤ 91º and the faulting process can be interpreted either as a fault with NNW-SSE orientation breaking up- or downdip or as N-S oriented fault breaking horizontally. From these, the first model agrees best with the result from the moment tensor inversion showing the event rupturing a most likely NW-SE oriented fault with a 78º fault dip towards northeast. Since the event at 19:52 UTC may rather have been a foreshock to the third event at 21:32 UTC than an aftershock of the first, it would be interesting to repeat the analysis for the latest event.
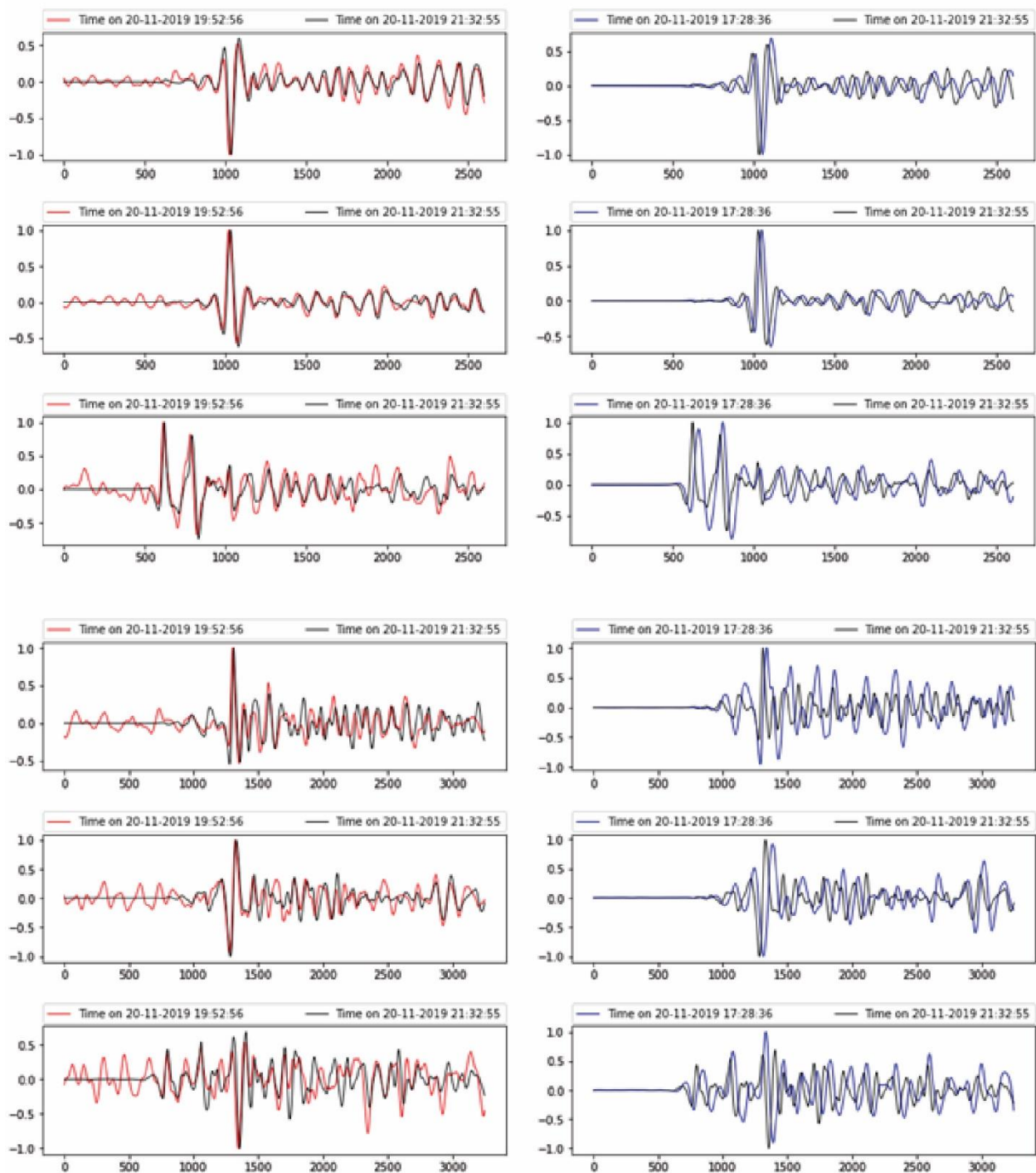
Figure 15: Comparison of waveforms, blue line: 17:28 UTC event, red line: 19:52 UTC event, black line: 21:32 UTC event, time axis in ms; top row: records of station DEEL (GR network), filtered between 0.01 and 2 Hz, traces shown on East, North and vertical component (from top to bottom within the same panel); bottom row: records of station MHW9S (BVEG network); left column: comparison between first and third event; right column: comparison between second and third event.

6. Administrative information

No bachelor, master or PhD theses have been produced during the course of the project. Project results have been presented at the following workshop and conference:

- "Application of a probabilistic moment tensor inversion to seismometer data recorded at North German gas fields" by D. Kühn, G. Richter, M. Rosskopf, G. Petersen, T. Dahm at AGIS Workshop, Hannover, Germany, November 2019.
- "Waveform-based probabilistic moment tensor inversion of shallow small-magnitude earthquakes (M<3.2) in North German gas fields" by D. Kühn, M. Rosskopf, G. Richter, J. A. López-Comino, G. Petersen, T. Dahm at IAGA-IASPEI Joint Scientific Assembly, Virtual Conference, 21-27 August 2021.

References

[1] Bischoff, M., Gestermann, N., Pasternak, M., Plenefisch, T., Schindewolf, A. (2020). Bericht zu den Erdbeben bei Kirchlinteln (Landkreis Verden) am 20. November 2019, M_L ≤ 3,2. Landesamt für Bergbau, Energie und Geologie & Bundesanstalt für Geowissenschaften und Rohstoffe.

[2] Bischoff, M., Gestermann, N., Pasternak, M., Plenefisch, T., Schindewolf, A. (2019). Bericht zu den Erdbeben bei Lastrup (LK Cloppenburg) im September und Oktober 2018, M_L ≤ 3,6. Landesamt für Bergbau, Energie und Geologie & Bundesanstalt für Geowissenschaften und Rohstoffe.

[3] Heimann, S., Isken, M., Kühn, D., Sudhaus, H., Steinberg, A., Vasyura-Bathke, H., Daout, S., Cesca, S., Dahm, T. (2018). Grond - A probabilistic earthquake source inversion framework. V. 1.0. GFZ Data Services. https://doi.org/10.5880/GFZ.2.1.2018.003

[4] Dost, B., van Stiphout, A., Kühn, D., Kortekaas, M., Ruigrok, E., Heimann, S. (2020). Probabilistic moment tensor inversion for hydrocarbon-induced seismicity in the Groningen gas field, the Netherlands, part 2: application. Bulletin of the Seismological Society of America, 110(5), 2112-2123.

[5] Kühn, D., Heimann, S., Isken, M. P., Ruigrok, E., Dost, B. (2020). Probabilistic moment tensor inversion for hydrocarbon-induced seismicity in the Groningen gas field, the Netherlands, part 1: testing. Bulletin of the Seismological Society of America, 110(5), 2095-2111.

[6] Petersen, G. M., Cesca, S., Kriegerowski, M., AlpArray Working Group. (2019). Automated quality control for large seismic networks: Implementation and application to the AlpArray seismic network. Seismological Research Letters, 90(3), 1177-1190.

[7] Heimann, S., M. Kriegerowski, M. Isken, S. Cesca, S. Daout, F. Grigoli, C. Juretzek, T. Megies, N. Nooshiri, A. Steinberg, Sudhaus, H., Vasyura-Bathke, H., Willey, T., Dahm, T. (2017). Pyrocko—An open-source seismology toolbox and library, https://doi.org/10.5880/GFZ.2.1.2017.001

[8] Heimann, S., H. Vasyura-Bathke, H. Sudhaus, M. Isken, M. Kriegerowski, A. Steinberg, T. Dahm (2019). A python framework for efficient use of pre-computed Green's functions in seismological and other physical forward and inverse source problems. Solid Earth 10(6), 1921–1935.

[9] Wang, R. (1999). A simple orthonormalization method for stable and efficient computation of Green's functions. Bulletin of the Seismological Society of America. 89(3), 733–741.

[10] Båth, M. (1965). Lateral inhomogeneities of the upper mantle, Tectonophysics, 2(6), 483–514.

[11] Kühn, D., Rosskopf, M., Richter, G. (2021). Analyse von Stationen des GRSN-Netzwerkes genutzt für Momententensorinversionen von Ereignissen in den norddeutschen Gasfeldern. DGMK project 819 technical report.

[12] Kühn, D., Rosskopf, M., Petersen, G., Richter, G. (2022). Analyse von Stationen des BVEG-

Netzwerkes genutzt für Momententensorinversionen von Ereignissen in den norddeutschen Gasfeldern. DGMK project 819 technical report.

[13] Peterson, J. R. (1993). Observations and modeling of seismic background noise. US Geological Survey Technical report no. 93-322.

[14] Peikert, D. (2016). 3D velocity model building Lower Saxony. DMT technical report.

[15] Reichert, J. C. (1993). Ein geophysikalischer Beitrag zur Erkundung der-Tiefenstruktur des Nordwestdeutschen Beckens längs-des refraktionsseismischen Profils Norddeutschland 1975/76. Geologisches Jahrbuch, E50, 3-87.

[16] Bassin, C., Laske, G. Masters, G. (2000). The Current Limits of Resolution for Surface Wave Tomography in North America. EOS Trans AGU, 81, F897.

[17] Aki, K (1957). Space and time spectra of stationary stochastic waves with special reference to microtremors. Bulletin of the Earthquake Research Institute, University of Tokyo, 35, 415–456.

[18] Okada, H. (2003). The microseismic survey method. Society of Exploration Geophysicists of Japan, translated by Koya Suto, Geophysical Monograph Series No. 12, Society of Exploration Geophysicists.

[19] Nogoshi, M., Igarashi, T. (1971). On the amplitude characteristics of microtremor (part 2). Journal of the Seismological Society of Japan, 24, 26–40.

[20] Tokimatsu, K. (1997). Geotechnical site characterization using surface waves. In: Ishihara, K. (ed), Proceedings of the 1st International Conference on Earthquake Geotechnical Engineering, Tokyo, Japan, 14–16 November 1995, 3, 1333–1368.

[21] Ibs von Seht, M., Wohlenberg, R. (1999). Microtremor measurements used to map thickness of soft soil sediments. Bulletin of the Seismological Society of America, 89, 250–259.

[22] SEISTER (2019). Analysis of consistency between B- and G-stations recorded for induced events in the Groningen gas field. Technical report, available from https://www.sodm.nl/binaries/staatstoezicht-op-de-mijnen/documenten/rapporten/2019/07/10/tussentijdse-rapportage-validatie-seismisch-netwerk-knmi-groningen/Bijlage+01B+STR_FUG_18P17_01_analysis_B-G_stations_Groningen_V2_Geredigeerd.pdf

[23] López-Comino, J. Á., Braun, T., Dahm, T., Cesca, S., Danesi, S. (2021). On the source parameters and genesis of the 2017, Mw 4 Montesano earthquake in the outer border of the Val d'Agri oilfield (Italy). Frontiers in Earth Science, 746.

www.dgmk.de